The Journal of Experimental Biology 206, 4191-4208

doi:10.1242/jeb.00663

Review

The aerodynamics of insect flight

Sanjay P. Sane

Department of Biology, University of Washington, Seattle, WA 98195, USA

(e-mail: sane@u.washington.edu)

Accepted 12 August 2003

Summary

The flight of insects has fascinated physicists and biologists for more than a century. Yet, until recently, researchers were unable to rigorously quantify the complex wing motions of flapping insects or measure the forces and flows around their wings. However, recent developments in high-speed videography and tools for computational and mechanical modeling have allowed researchers to make rapid progress in advancing our understanding of insect flight. These mechanical and computational fluid dynamic models, combined with modern flow visualization techniques, have revealed that the fluid dynamic phenomena underlying flapping flight are different from those of non-flapping, 2-D wings on which most previous models were based. In particular, even at high angles of attack, a prominent leading edge vortex remains stably attached on the insect wing and does not shed into an unsteady wake, as would be expected from non-flapping 2-D wings. Its presence greatly enhances the forces generated by the wing, thus enabling insects to hover or maneuver. In addition, flight forces are further enhanced by other mechanisms acting during changes in angle of attack, especially at stroke reversal, the mutual interaction of the two wings at dorsal stroke reversal or wing–wake interactions following stroke reversal. This progress has enabled the development of simple analytical and empirical models that allow us to calculate the instantaneous forces on flapping insect wings more accurately than was previously possible. It also promises to foster new and exciting multi-disciplinary collaborations between physicists who seek to explain the phenomenology, biologists who seek to understand its relevance to insect physiology and evolution, and engineers who are inspired to build micro-robotic insects using these principles. This review covers the basic physical principles underlying flapping flight in insects, results of recent experiments concerning the aerodynamics of insect flight, as well as the different approaches used to model these phenomena.

Key words: insect flight, aerodynamics, Kramer effect, delayed stall, quasi-steady modeling, flapping flight, kinematics, forces, flows, leading edge vortex.

Introduction

Insects owe much of their extraordinary evolutionary success to flight. Compared with their flightless ancestors, flying insects are better equipped to evade predators, search food sources and colonize new habitats. Because their survival and evolution depend so crucially on flight performance, it is hardly surprising that the flight-related sensory, physiological, behavioral and biomechanical traits of insects are among the most compelling illustrations of adaptations found in nature. As a result, insects offer biologists a range of useful examples to elucidate both structure–function relationships and evolutionary constraints in organismal design (Brodsky, 1994; Dudley, 2000).

Insects have also stimulated a great deal of interest among physicists and engineers because, at first glance, their flight seems improbable using standard aerodynamic theory. The small size, high stroke frequency and peculiar reciprocal flapping motion of insects have combined to thwart simple ‘back-of-the-envelope’ explanations of flight aerodynamics. As with many problems in biology, a deep understanding of insect flight depends on subtle details that might be easily overlooked in otherwise thorough theoretical or experimental analyses. In recent years, however, investigators have benefited greatly from the availability of high-speed video for capturing wing kinematics, new methods such as digital particle image velocimetry (DPIV) to quantify flows, and powerful computers for simulation and analysis. Using these and other new methods, researchers can proceed with fewer simplifying assumptions to build more rigorous models of insect flight. It is this more detailed view of kinematics, forces and flows that has led to significant progress in our understanding of insect flight aerodynamics.

Experimental challenges

Because of their small size and high wing beat frequencies, it is often quite difficult to quantify the wing motions of free-

flying insects. For example, an average-sized insect such as the common fruit fly *Drosophila melanogaster* is approximately 2–3 mm in length and flaps its wings at a rate of 200 Hz. Just the mere quantification of motion for such small and fast-moving wings continues to pose significant challenges to current technology. Early attempts to capture free-flight wing kinematics such as Ellington's comprehensive and influential survey (Ellington, 1984c) relied primarily on single-image high-speed cine. Although quite informative, especially because film continues to offer exceptional spatial resolution, single-view techniques cannot provide an accurate time course of the angle of attack of the two wings. More recent methods have employed high-speed videography (Willmott and Ellington, 1997b), which offers greater light sensitivity and ease of use, albeit at the cost of image resolution. A further consideration is that insects rely extensively on visual feedback, and hence care must be taken to ensure that lighting conditions do not significantly impair an insect's behavior.

Even more challenging than capturing wing motion in 3-D is measuring the time course of aerodynamic forces during the stroke. At best, flight forces have been measured on the body of the insect rather than its wings, making it very difficult to separate the inertial forces from the aerodynamic forces generated by each wing (Cloupeau et al., 1979; Buckholz, 1981; Somps and Luttges, 1985; Zanker and Gotz, 1990; Wilkin and Williams, 1993). In addition, tethering can alter the wing motion, and thus forces produced, as compared with free-flight conditions. Researchers have overcome these limitations using two strategies. The first method involves constructing dynamically scaled models on which it is easier to directly measure aerodynamic forces and visualize flows (Bennett, 1970; Maxworthy, 1979; Spedding and Maxworthy, 1986; Dickinson and Götz, 1993; Sunada et al., 1993; Ellington et al., 1996; Dickinson et al., 1999). A second approach is to construct computational fluid dynamic simulations of flapping insect wings (Liu et al., 1998; Liu and Kawachi, 1998; Wang, 2000; Ramamurti and Sandberg, 2002; Sun and Tang, 2002). The power of both these approaches, however, depends critically on accurate knowledge of wing motion.

Conventions and terminology

Because most literature on flapping flight has adopted standard terminology borrowed from fixed wing aerodynamics, it is necessary to first develop a nomenclature that allows us to unambiguously distinguish between these two types of flight. As in fixed wing aerodynamics, 'wing span' refers to the length between the tips of the wings when they are stretched out laterally (Fig. 1A), whereas 'wing length' refers to the base-to-tip length of one wing. Wing span is often given as twice wing length, thereby ignoring the width of the animal's thorax. 'Wing chord' refers to the section between the leading and trailing edge of the wing at any given position along the span (Fig. 1A). The ratio of span to mean chord is an important non-dimensional morphological parameter termed 'aspect ratio'. 'Angle of attack' refers to the angle that the wing chord makes with the relative velocity vector of the fluid far away from the influence of the airfoil, i.e. relative to the 'far-field flow' or 'free-stream flow' (Fig. 1B). The restriction to far-field flow in this definition is necessary because the presence of the airfoil influences the fluid field immediately around it. In all real airfoils, the process of generating lift creates an induced downwash in the flow all around the wing. Although the magnitude of this downwash (U') is small compared with the 'free-stream velocity' (U_∞), it can significantly alter the direction of resultant velocity and thus attenuate the performance of the wing by lowering the angle of attack (Fig. 1B; Munk, 1925a; Kuethe and Chow, 1998). For this reason, it is important to qualify whether the angle of attack is measured with respect to the gross flow in the immediate vicinity of the wing or far away from it. The angle of attack relative to the direction of free-stream velocity is called 'geometric angle of attack' (α), whereas the altered angle of attack relative to the locally deflected free stream is called the 'aerodynamic' or 'effective angle of attack' (α'), where:

$$\alpha - \alpha' = \tan^{-1}\left(\frac{U'}{U_\infty}\right). \quad (1)$$

Because it is difficult to physically measure the downwash-related deflection of the free stream, most insect flight studies report geometric rather than aerodynamic angles of attack.

From one stroke to the next, insects rapidly alter many kinematic features that determine the time course of flight forces, including stroke amplitude, angle of attack, deviation from mean stroke plane, wing tip trajectory and wing beat frequency (Ennos, 1989b; Ruppell, 1989), as well as timing and duration of wing rotation during stroke reversal (Srygley and Thomas, 2002). Moreover, they may vary these parameters on each wing independently to carry out a desired maneuver. Hence, it is misleading to lump all patterns of insect wing motion into a single simple pattern. Mindful of this vast diversity in wing kinematics patterns, the wing motion of insects may be divided into two general patterns of flapping. Most researchers have restricted their studies to hovering because it is more convenient mathematically to calculate the force balance by equating lift and weight in this case. While hovering, most insects move their wings back and forth in a roughly horizontal plane, whereas others use a more inclined plunging stroke (Ellington, 1984c; Dudley, 2000). Despite the predominance of the back-and-forth pattern, the terms 'upstroke' and 'downstroke' are used conventionally to describe the ventral-to-dorsal and dorsal-to-ventral motion of the wing, respectively. It is important to note that as insects fly forward, their stroke plane becomes more inclined forward. The term 'wing rotation' will generally refer to any change in angle of attack around a chordwise axis. During the downstroke-to-upstroke transition, the wing 'supinates' rapidly, a rotation that brings the ventral surface of the wing to face upward. The wing 'pronates' rapidly at the end of the upstroke, bringing the ventral surface to face downward (Fig. 1C).

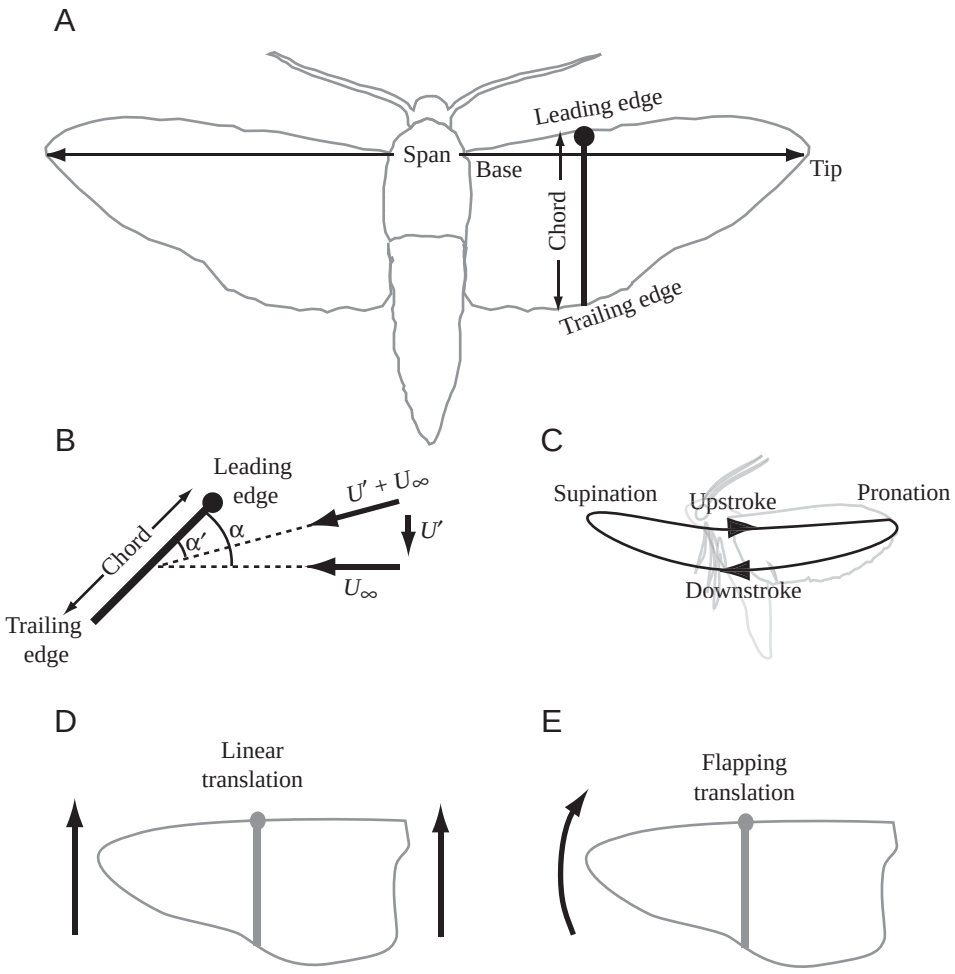

Fig. 1. Conventions and terminology. (A) Sketch of an insect. The wing section is depicted by a segment drawn perpendicular to a line joining the wing base and wing tip. This segment, representing the wing chord, connects the leading edge (filled circle) to the trailing edge. (B) Sectional view of the insect wing. The free-stream velocity is denoted by U_∞, and downwash velocity is denoted by U' (written in bold to signify their vector nature). The geometric angle of attack (α) is the angle that the wing section makes with U_∞. The aerodynamic angle of attack (α') is given by the angle between the wing section and the free-stream velocity deflected as a result of the downwash. (C) Phases of insect wing kinematics. Wing pronation occurs dorsally as the wing transitions from upstroke to downstroke, and wing supination occurs ventrally at the transition from downstroke to upstroke. (D,E) Linear *vs* flapping translation. In a linearly translating wing (D), both wing tip and base translate at the same velocity, whereas in a flapping translating wing (E), the tip rotates around an axis fixed at the base.

In the present review, 'linear (or non-flapping) translation' will refer to airfoils translating linearly (Fig. 1D), whereas 'flapping translation' will refer to an airfoil revolving around a central axis (Fig. 1E). Since much of the theoretical literature addresses the aerodynamic performance of idealized 2-D sections of wings, it is important to distinguish between finite and infinite wings. The term 'finite wing' refers to an actual 3-D wing with two tips and thus a finite span length. From the perspective of fluid mechanics, the importance of the wing tips is that they create component of fluid velocity that runs along the span of the wing, perpendicular to the direction of far-field flow during linear translation. By contrast, 'infinite wings' are theoretical abstractions of 2-D structures that can only create chord-wise flow. Such wings are experimentally realized by closely flanking the tips of the wings with rigid walls that limit span-wise flow, thus constraining the fluid to move in two dimensions. It is also important to note that, by definition, a 2-D wing cannot perform flapping motions. Nevertheless, 2-D formulations based on an infinite wing assumption have often proved very useful in the study of animal flight and are particularly relevant in cases where wings have a high aspect ratio.

Within the context of force and flow dynamics, the term 'steady' signifies explicit time independence, whereas the word 'unsteady' signifies explicit temporal evolution due to inherently time-dependent phenomena within the fluid. In flapping flight, steady does not necessarily imply time invariant. Forces on airfoils may change with time without being explicitly dependent on time, simply because the underlying motion of the airfoils varies. If the forces at each instant are modeled by the assumption of inherently time-independent fluid dynamic mechanisms, then such a model is called 'quasi-steady', i.e. steady at each instant but varying with time due to kinematic time dependence.

Background theory for thin airfoils

Before addressing the specific theoretical challenges posed by insect flight aerodynamics, it is first necessary to introduce general equations and physical principles that govern forces and flows created by moving objects submersed in fluids. These formulations borrow extensively from methods used by physicists and engineers for nearly 100 years to predict the forces created by thin flat wings moving at very low angles of attack (Prandtl and Tietjens, 1957b; Milne-Thomson, 1966).

Unless otherwise mentioned, the theory in this section applies to 2-D airfoils moving in incompressible fluids. Also, in the analysis that follows, most key physical parameters

appear as non-dimensional entities. Non-dimensional forms of equations are scale-invariant, thereby making it possible to compare flows across a wide range of scales. Although any reasonable scheme of non-dimensionalizing parameters is valid for the purpose of this review, the scheme conventionally used is the one developed by Ellington (1984b–e) for the purpose of insect flight aerodynamics. For more detailed treatments of the physical concepts, the reader is referred to classic fluid dynamics texts written by Lamb (1945), Landau and Lifshitz (1959), Milne-Thomson (1966) and Batchelor (1973) and books focusing on thin airfoil theory, such as Glauert (1947) and Prandtl and Tietjens (1957b).

The fluid motion around an insect wing, like any other submersed object, is adequately described by the incompressible Navier–Stokes equation, a non-dimensional form of which can be written as:

$$\frac{\partial \hat{\mathbf{u}}}{\partial \hat{t}} + (\hat{\mathbf{u}} \cdot \hat{\nabla})\hat{\mathbf{u}} = -\hat{\nabla}\hat{P} + \frac{1}{Re}\hat{\nabla}^2\hat{\mathbf{u}}, \quad (2)$$

where $\hat{\mathbf{u}}$, $\hat{t}$, $\hat{P}$ are, respectively, the velocity of the flapping wing relative to its fluid medium, time and pressure. All these quantities are non-dimensionalized (denoted by ^) with respect to their corresponding 'characteristic' measures. The choice of a characteristic measure is somewhat arbitrary and often based on the physicist's intuition of which constants of the system are physically meaningful. For example, when modeling the flow around a section of a high aspect ratio wing, the chord length is often used as the characteristic length measure. The operator:

$$\hat{\nabla} = \frac{\partial}{\partial \hat{x}}\mathbf{i} + \frac{\partial}{\partial \hat{y}}\mathbf{j} + \frac{\partial}{\partial \hat{z}}\mathbf{k}, \quad (3)$$

is a non-dimensional form of the vector 'del' operator, and **i**, **j** and **k** are unit Cartesian vectors. The left-hand side of equation 2 represents the Lagrangian (or material) derivative of the velocity, incorporating both the implicit and explicit dependence on time. In the Eulerian representation, the Lagrangian derivative is simply the temporal derivative of the motion of a fluid particle as measured by an observer moving with the fluid. The denominator of the last term in equation 2 is the Reynolds number (*Re*), a non-dimensional parameter that describes the ratio of inertia of a moving fluid mass to the viscous dissipation of its motion. Reynolds number can be calculated by the relation $Re=(\rho U_\infty L)/\eta$, where ρ is the density of the fluid medium, U_∞ is the velocity of the fluid relative to the moving object, L is a characteristic length measure and η is the dynamic viscosity of the fluid medium. This parameter roughly characterizes the fluid dynamic regime in which an insect operates from laminar (for low values of *Re*) to turbulent (for high values of *Re*). When viscosity is large, *Re* is small and the last term in equation 2 becomes relatively more important than the pressure term. When viscosity is negligible, the values of *Re* are large and the last term can be dropped from the equation to obtain the inviscid form (i.e. zero viscosity) of equation 2, usually called the 'Euler equation'. Equation 2 also provides the mathematical justification for the use of dynamically scaled physical models. The non-dimensionalized forces and flows generated by isometrically scaled objects are the same provided that the *Re* are identical.

The Navier–Stokes equation provides the fundamental theoretical basis for simulating forces and flows from arbitrary or measured kinematics. It is not, however, easy to use in an experimental context, because it is quite difficult to measure the pressure field in the space around a wing. An alternative and sometimes more convenient form of the Navier–Stokes equation may be derived by taking the curl of both sides in equation 2. This eliminates the pressure term because the curl of a gradient vanishes, and the equation simplifies to:

$$\frac{\partial \hat{\boldsymbol{\omega}}}{\partial \hat{t}} = \hat{\nabla} \times (\hat{\mathbf{u}} \times \hat{\boldsymbol{\omega}}) + \frac{1}{Re}\hat{\nabla}^2\hat{\boldsymbol{\omega}}. \quad (4)$$

The quantity $\hat{\boldsymbol{\omega}}=\hat{\nabla}\times\hat{\mathbf{u}}$, defined as the 'vorticity' of the fluid, is very useful in the conceptualization and characterization of the flows around airfoils. For the case of steady inviscid flows, $\hat{\boldsymbol{\omega}}=0$ and the flows are said to be 'irrotational'. When flows are irrotational over all space, it is often convenient to express the velocity field as a gradient of a scalar potential function Φ (i.e. $\hat{\mathbf{u}}=\hat{\nabla}\Phi$). This approach, called the 'potential theory', has proven very useful in the elucidation of many basic aerodynamic theorems. Essentially, the technique involves constructing specific forms of Φ that best describe a given fluid dynamic phenomenon under its appropriate initial and boundary conditions. Vorticity arises from a combination of mutually orthogonal spatial derivatives of velocity at a given point in space. Thus, its value at any given point does not offer a complete picture of the related aerodynamic forces. To calculate aerodynamic forces, small vorticity elements must be integrated over a surface area around an airfoil. Using the Stokes theorem, which relates the area integral of normal component of vorticity to a line integral of velocity around a closed contour Σ bounding a surface S:

$$\oint_{\Sigma} \hat{\mathbf{u}} \cdot d\hat{\mathbf{l}} = \iint \hat{\boldsymbol{\omega}} \cdot \hat{\mathbf{n}}\, d\hat{S}. \quad (5)$$

The quantity on the left-hand side of this equation is defined as 'circulation' (often denoted by Γ). For potential flows, its value around any closed contour not enclosing a wing section is zero because vorticity is zero everywhere in accordance with the assumption of irrotational flow. However, if the closed contour encloses a wing section, then the presence of even the slightest viscosity, and therefore a finite amount of shear at the wing-fluid interface, will give rise to finite vorticity and thus non-zero circulation.

Under completely inviscid conditions, one would expect the fluid to deflect only minimally by the presence of an airfoil, thereby generating a flow field around the wing similar to the one described in Fig. 2A. Under such conditions, the rear stagnation point (where velocity is zero) would be present not at the tip of the trailing edge but on the upper surface of the

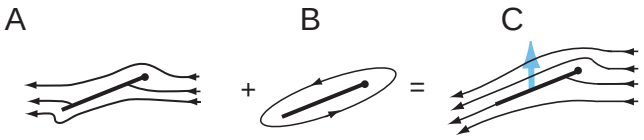

Fig. 2. Kutta condition and circulation. The Kutta condition arises from a sum of the flow around an airfoil placed in an inviscid fluid (A) to additional circulation arising from the presence of viscosity (B) to yield a smooth, tangential flow from the trailing edge (C). When satisfied, the Kutta condition ensures that the vorticity generated at the trailing edge is zero. For the inviscid case, the net force on the airfoil (blue arrow) acts perpendicular to the free stream.

wing. However, to maintain this flow profile, the fluid must turn sharply around the trailing edge causing a singularity or 'kink' in the flow at the trailing edge. Such a flow profile necessitates a high gradient in velocity at the trailing edge, thereby causing high viscous forces due to shear. The viscous forces in turn will eventually eradicate this singularity. Thus, the presence of even the slightest viscosity in the fluid functions to smooth out sharp gradients in flow. This phenomenon may be incorporated into an otherwise inviscid formulation by adding a circulatory component to the flow field (Fig. 2B). At a unique value of the additional circulation, the stagnation point is stationed exactly at the trailing edge. When this condition is met, the fluid stream over the plate meets the fluid stream under the plate smoothly and tangentially at the trailing edge (Fig. 2C). This phenomenon is called the 'Kutta condition', which ensures that the slopes of the fluid streams above and below the wing surface are equal, and thus the vorticity (i.e. curl of the velocity) at the trailing edge is zero. In addition, when satisfied, the Kutta condition ensures that the inclined plate imparts a downward momentum to the fluid. This, in essence, is the classic Kutta–Jukowski theory of thin airfoils (Kuethe and Chow, 1998). For ideal fluids, the net force acts perpendicular to the direction of motion with no component in the plane of motion. Thus, this theory predicts zero resistance in the direction of motion (or 'drag') for airfoils moving through fluids at small angles of attack (called D'Alembert's paradox). However, in the presence of even the smallest amount of shear, the net force vector is tilted backward, i.e. normal to the wing. Even at reasonably high *Re*, the net aerodynamic force on the wing surface is usually perpendicular to the surface of the inclined wing rather than to the direction of motion. The non-zero component of this force normal to fluid motion is defined as 'lift', and the component parallel to the fluid motion is defined as 'profile drag'. The component of drag due to viscous shear along the surface on an airfoil is called 'viscous drag'.

Far from the airfoil, the behavior of the fluid is similar to that expected by potential flow theory. For this reason, although the fluid is not actually irrotational, potential theory can be used to conveniently describe such situations as long as the Kutta condition is satisfied. For steady inviscid flows, the Kutta–Jukowski theorem relates circulation, and therefore vorticity, around an airfoil to forces by the equation:

$$\hat{L}' = \oint_{\Sigma} \hat{\mathbf{u}} \cdot d\hat{\mathbf{l}} \,. \tag{6}$$

Note that lift can also be related to vorticity using equation 5. In equation 6, $\hat{L}'$ is the lift per unit span non-dimensionalized with respect to the product of density of the fluid (ρ), mean chord length, and the square of free-stream velocity of the fluid (U_∞). This quantity (conventionally multiplied by two) is called the 'lift coefficient' and is usually denoted in literature by C_L. Similarly, the non-dimensional drag is called the 'drag coefficient' and is usually denoted by C_D. For inviscid fluids undergoing steady (non-accelerated) flows,

$$\frac{d}{dt} \oint_{\Sigma} \hat{\mathbf{u}} \cdot d\hat{\mathbf{l}} = 0 \,, \tag{7}$$

or

$$\oint_{\Sigma} \hat{\mathbf{u}} \cdot d\hat{\mathbf{l}} = \text{constant} \,. \tag{8}$$

When an airfoil starts from rest, the net circulation in the fluid before the start of the motion is zero. Thus, equation 8 is simply a mathematical expression for Kelvin's law, which states that the total circulation (and the total vorticity) in an ideal fluid must remain zero at all times. In other words, if new vorticity (or circulation) is introduced in an inviscid fluid (e.g. through an application of the Kutta condition), then it must be accompanied by equal and opposite vorticity.

Physically, because the presence of viscosity disallows infinite shear, the fluid immediately abounding the airfoil is stationary with respect to the airfoil. This condition, called the 'no-slip condition', is an important boundary condition in most analytical treatments of airfoils. Due to the no-slip condition, a continuous layer forms over the airfoil across which the velocity of the fluid goes from zero (for the stationary layer adjoining the body) to its maximum value (corresponding to the free-stream flow). Such regions are called 'boundary layers' and their thickness depends on the Reynolds number of the flow (Schlichting, 1979). Another boundary condition arises from the requirement that the normal velocity of the fluid on the surface of the airfoil must be zero. This condition is sometimes called the 'no penetration' condition. These boundary conditions apply at the interface of solids and fluids. In free fluids, however, conditions may often arise where the tangential, but not the normal, component of velocity is discontinuous across two adjacent layers. Such interfaces have high vorticity and are called 'vortex sheets', or 'vortex lines' for the two-dimensional case.

When a volume element dV of the fluid has non-zero vorticity $\boldsymbol{\omega}$, it induces a velocity $\mathbf{v}$ at a distance r in the neighboring region. The expression to calculate this velocity is given by (in dimensional form):

$$\mathbf{v} = \frac{1}{4\pi} \int_{V} \boldsymbol{\omega} \times \frac{\mathbf{r}}{r^3} \, dV \,, \tag{9}$$

where **r** is the displacement vector or distance vector. This is called the Biot-Savart's law (Milne-Thomson, 1966), which, like its electromagnetic analog, is an inverse square relationship. This integral must be evaluated over the entire volume of the fluid (V). Equation 9 is very useful in most vorticity-based analyses of fluid dynamics, as well as in modeling the effects of vortex dipoles on their surrounding medium.

The solenoidal (i.e. zero divergence) nature of vorticity fields enables vorticity-based methods to define very useful kinematic quantities called 'moments of vorticity'. These quantities are useful because their values are independent of the conditions in the interior of a boundary surrounding the region of interest since no new vorticity can be generated within a fluid subject to conservative external forces. Instead, vorticity is generated at the solid–fluid boundary and diffuses into the fluid medium (Truesdell, 1954). Of particular utility is the first moment of vorticity because it can be related to aerodynamic forces. This quantity is given by:

$$\boldsymbol{\gamma} = \int_R \mathbf{r} \times \boldsymbol{\omega}\, dR, \tag{10}$$

where **r** is the distance from origin of an arbitrary co-ordinate system moving with the free stream, ω is the vorticity and R is the area of region of interest encompassing all vorticity elements. For the two-dimensional incompressible viscous case, the sectional aerodynamic force **F** may be derived from the first moment of vorticity **γ** by the equation:

$$\mathbf{F} = -\rho \frac{d\boldsymbol{\gamma}}{dt} + \rho \frac{d}{dt} \int_S \boldsymbol{\nu}\, dA, \tag{11}$$

where ρ is fluid density, A is the cross-sectional area of the airfoil and **ν** is the velocity of a point within the airfoil (Wu, 1981). The first term on the right-hand side of this equation represents the temporal derivative of the first moment of vorticity, which is equal to the force arising from the vorticity created by the movement of the airfoil. The second term in the equation represents the inertial force of the fluid displaced by the wing section. For an infinitesimally thin wing, the sectional area is negligible and force depends solely on the moment of vorticity. For the simple case of any bound circulation, a stable distribution of vorticity moves with the wing, and a constant growth of the moment of vorticity results solely from the wing's motion. In agreement with the Kutta–Jukowski theorem, the sectional lift is equal to the product of the circulation created by a wing and its translational velocity (Wu, 1981). Equation 11 is more general, however, and can account for forces generated when both the strength and distribution of vorticity around the wing are changing, as might occur at the start of motion, during rapid changes in kinematics or when the wing encounters vorticity created by its own wake or that of another wing.

Theoretical challenges

The challenges in adopting the traditional methods described in the previous section to insect flight are manifold and only briefly described here. Determined primarily by their variation in size, flying insects operate over a broad range of Reynolds numbers from approximately 10 to 10^5 (Dudley, 2000). For comparison, the Reynolds number of a swimming sperm is approximately 10^{-2}, a swimming human being is 10^6 and a commercial jumbo jet at 0.8 Mach is 10^7. At the high Reynolds numbers characteristic of the largest insects, the importance of the viscous term in equation 2 may be negligible and, as with aircraft, flows and forces may be governed by its inviscid form (the Euler equation). Such simplifications may not always be possible for most species, whose small size translates into low Reynolds numbers. This is not to say that viscous forces dominate in small insects. To the contrary, even at a Reynolds number of 10, inertial forces are roughly an order of magnitude greater than viscous forces. However, viscous effects become more important in structuring flow and thus cannot be ignored. Due to these viscous effects, the principles underlying aerodynamic force production may differ in small *vs* large insects. For tiny insects, small perturbations in the fluid may be more rapidly dissipated due to viscous resistance to fluid motion. However, for larger insects operating at higher Reynolds numbers, small perturbations in the flow field accumulate with time and may ultimately result in stronger unsteadiness of the surrounding flows. Even with the accurate knowledge of the smallest perturbations, such situations are impossible to predict analytically because there may be several possible solutions to the flow equations. In such cases, strict static and dynamic initial and boundary conditions must be identified to reduce the number of solutions to a few meaningful possibilities.

Analytical models of insect flight

The experimental and theoretical challenges mentioned in the previous sections constrained early models of insect flight to analysis of far-field wakes rather than the fluid phenomena in the immediate vicinity of the wing. Although such far-field models could not be used to calculate the instantaneous forces on airfoils, they offered some hope of characterizing average forces as well as power requirements. Most notable among these are the 'vortex models' (Ellington, 1978, 1980, 1984e; Rayner, 1979a,b), both of which are derived by approximating flapping wings to blades of a propeller or, more accurately, to idealized actuator disks that generate uniform pressure pulses to impart downward momentum to the surrounding fluid. By this method, the mean lift required to hover may be estimated by equating the rate of change of momentum flux within the downward jet with the weight of the insect and thus calculating the circulation required in the wake to maintain this force balance. A detailed description of these theories appears in Rayner (1979a,b) and Ellington (1984e) and is beyond the scope of this review, which will focus instead on near-field models.

Despite the caveats presented in the last section, a few researchers have been able to construct analytical near-field

models for the aerodynamics of insect flight with some degree of success. Notable among these are the models of Lighthill (1973) for the Weis-Fogh mechanism of lift generation (also called clap-and-fling), first proposed to explain the high lift generated in the small chalcid wasp *Encarsia formosa*, and that of Savage et al. (1979) based on an idealized form of Norberg's kinematic measurements on the dragonfly *Aeschna juncea* (Norberg, 1975). Although both these models were fundamentally two dimensional and inviscid (albeit with some adjustments to include viscous effects), they were able to capture some crucial aspects of the underlying aerodynamic mechanisms. Specifically, Lighthill's model of the fling (Lighthill, 1973) was qualitatively verified by the empirical data of Maxworthy (1979) and Spedding and Maxworthy (1986). Similarly, the model of Savage et al. (1979) was able to make specific predictions about force enhancement during specific phases of kinematics (e.g. force peaks observed as the wings rotate prior to supination) that were later confirmed by experiments (Dickinson et al., 1999; Sane and Dickinson, 2002). In studies on dragonflies and damselflies, the 'local circulation method' was also used with some degree of success (Azuma et al., 1985; Azuma and Watanabe, 1988; Sato and Azuma, 1997). This method takes into account the spatial (along the span) and temporal changes in induced velocity and estimates corrections in the circulation due to the wake. The more recent analytical models (e.g. Zbikowski, 2002; Minotti, 2002) have been able to incorporate the basic phenomenology of the fluid dynamics underlying flapping flight in a more rigorous fashion, as well as take advantage of a fuller database of forces and kinematics (Sane and Dickinson, 2001).

Computational fluid dynamics (CFD)

With recent advances in computational methods, many researchers have begun exploring numerical methods to resolve the insect flight problem, with varying degrees of success (Smith et al., 1996; Liu et al., 1998; Liu and Kawachi, 1998; Wang, 2000; Ramamurti and Sandberg, 2002; Sun and Tang, 2002). Although ultimately these techniques are more rigorous than simplified analytical solutions, they require large computational resources and are not as easily applied to large comparative data sets. Furthermore, CFD simulations rely critically on empirical data both for validation and relevant kinematic input. Nevertheless, several collaborations have recently emerged that have led to some exciting CFD models of insect flight.

One such approach involved modeling the flight of the hawkmoth *Manduca sexta* using the unsteady aerodynamic panel method (Smith et al., 1996), which employs the potential flow method to compute the velocities and pressure on each panel of a discretized wing under the appropriate boundary conditions. Also using *Manduca* as a model, Liu and co-workers were the first to attempt a full Navier–Stokes simulation using a 'finite volume method' (Liu et al., 1998; Liu and Kawachi, 1998). In addition to confirming the smoke streak patterns observed on both real and dynamically scaled model insects (Ellington et al., 1996), this study added finer detail to the flow structure and predicted the time course of the aerodynamic forces resulting from these flow patterns. More recently, computational approaches have been used to model *Drosophila* flight for which force records exist based on a dynamically scaled model (Dickinson et al., 1999). Although roughly matching experimental results, these methods have added a wealth of qualitative detail to the empirical measurements (Ramamurti and Sandberg, 2002) and even provided alternative explanations for experimental results (Sun and Tang, 2002; see also section on wing–wake interactions). Despite the importance of 3-D effects, comparisons of experiments and simulations in 2-D have also provided important insight. For example, the simulations of Hamdani and Sun (2001) matched complex features of prior experimental results with 2-D airfoils at low Reynolds number (Dickinson and Götz, 1993). Two-dimensional CFD models have also been useful in addressing feasibility issues. For example, Wang (2000) demonstrated that the force dynamics of 2-D wings, although not stabilized by 3-D effects, might still be sufficient to explain the enhanced lift coefficients measured in insects.

Quasi-steady modeling of insect flight

In the hope of finding approximate analytical solutions to the insect flight problem, scientists have developed simplified models based on the quasi-steady approximations. According to the quasi-steady assumption, the instantaneous aerodynamic forces on a flapping wing are equal to the forces during steady motion of the wing at an identical instantaneous velocity and angle of attack (Ellington, 1984a). It is therefore possible to divide any dynamic kinematic pattern into a series of static positions, measure or calculate the force for each and thus reconstruct the time history of force generation. By this method, any time dependence of the aerodynamic forces arises from time dependence of the kinematics but not that of the fluid flow itself. If such models are accurate, then it would be possible to use a relatively simple set of equations to calculate aerodynamic forces on insect wings based solely on knowledge of their kinematics.

Although quasi-steady models had been used with limited success in the past (Osborne, 1950; Jensen, 1956), they generally appeared insufficient to account for the necessary mean lift in cases where the average flight force data are available. In a comprehensive review of the insect flight literature, Ellington (1984a) used the logic of 'proof-by-contradiction' to argue that if even the maximum predicted lift from the quasi-steady model was less than the mean lift required to hover, then the model had to be insufficient. Conversely, if the maximum force calculated from the model was greater than or equal to the mean forces required for hovering, then the quasi-steady model cannot be discounted. Based on a wide survey of data available at the time, he convincingly argued that in most cases the existing quasi-steady theory fell short of calculating even the required average

lift for hovering, and a substantial revision of the quasi-steady theory was therefore necessary (Ellington, 1984a). He further proposed that the quasi-steady theory must be revised to include wing rotation in addition to flapping translation, as well as the many unsteady mechanisms that might operate. Since the Ellington review, several researchers have provided more data to support the insufficiency of the quasi-steady model (Ennos, 1989a; Zanker and Gotz, 1990; Dudley, 1991). These developments have spurred the search for specific unsteady mechanisms to explain the aerodynamic forces on insect wings.

Physical modeling of insect flight

Given the difficulties in directly studying insects or making theoretical calculations of their flight aerodynamics, many researchers have used mechanical models to study insect flight. When constructing these models, the Reynolds number and reduced frequency parameter (body velocity/wing velocity) of the mechanical model is matched to that of an actual insect. This condition, called 'dynamic scaling', ensures that the underlying fluid dynamic phenomena are conserved. Because it is relatively easier to measure and visualize flow around the scaled models than on insect wings, such models have proved extremely useful in identification and analysis of several unsteady mechanisms such as the clap-and-fling (Bennett, 1977; Maxworthy, 1979; Spedding and Maxworthy, 1986), delayed stall (Dickinson and Götz, 1993; Ellington et al., 1996), rotational lift (Bennett, 1970; Ellington, 1984d; Dickinson et al., 1999; Sane and Dickinson, 2002) and wing–wake interactions (Dickinson, 1994; Dickinson et al., 1999). These various mechanisms are discussed in the following section.

Unsteady mechanisms in insect flight

Wagner effect

When an inclined wing starts impulsively from rest, the circulation around it does not immediately attain its steady-state value (Walker, 1931). Instead, the circulation rises slowly to the steady-state estimate (Fig. 3). This delay in reaching the steady-state values may result from a combination of two phenomena. First, there is inherent latency in the viscous action on the stagnation point and thus a finite time before the establishment of Kutta condition. Second, during this process, vorticity is generated and shed at the trailing edge, and the shed vorticity eventually rolls up in the form of a starting vortex. The velocity field induced in the vicinity of the wing by the vorticity shed at the trailing edge additionally counteracts the growth of circulation bound to the wing. After the starting vortex has moved sufficiently far from the trailing edge, the wing attains its maximum steady circulation (Fig. 3). This sluggishness in the development of circulation was first proposed by Wagner (1925) and studied experimentally by Walker (1931) and is often referred to as the Wagner effect. Unlike the other unsteady mechanisms described below, the Wagner effect is a phenomenon that would act to attenuate

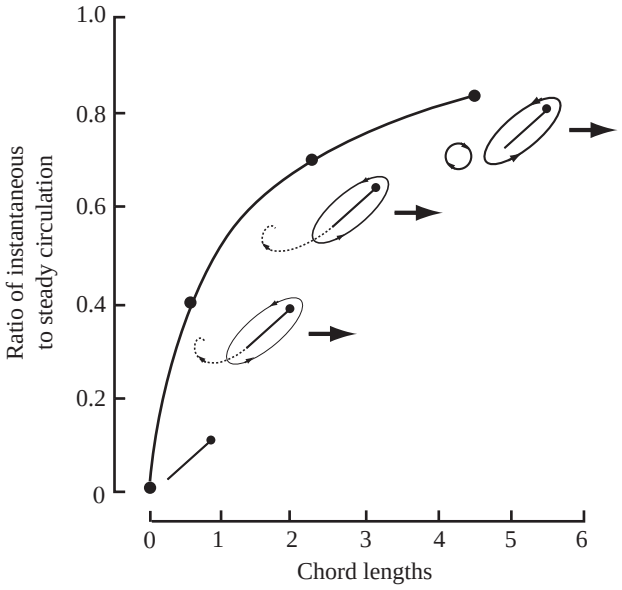

Fig. 3. Wagner effect. The ratio of instantaneous to steady circulation (*y*-axis) grows as the trailing edge vortex moves away from the airfoil (inset), and its influence on the circulation around the airfoil diminishes with distance (*x*-axis). Distance is non-dimensionalized with respect to chord lengths traveled. The graph is based on fig. 35 in Walker (1931). The inset figures are schematic diagrams of the Wagner effect. Dotted lines show the vorticity shedding from the trailing edge, eventually rolling up into a starting vortex. As this vorticity is shed into the wake, bound circulation builds up around the wing section, shown by the increasing thickness of the line drawn around the wing section.

forces below levels predicted by quasi-steady models. However, more recent studies with 2-D wings (Dickinson and Götz, 1993) indicate that the Wagner effect might not be particularly strong at the Reynolds numbers typical of most insects. For infinite wings translating at small angles of attack (less than 10°), lift grows very little, if at all, after two chord lengths of travel. Similar experiments for flapping translation in 3-D also show little evidence for the Wagner effect (Dickinson et al., 1999). However, because this effect relates directly to the growth of vorticity at the onset of motion, both its measurement and theoretical treatment are complicated due to interaction with added mass effects described in a later section. Nevertheless, most recent models of flapping insect wings have neglected the Wagner effect (but see Walker and Westneat, 2000; Walker, 2002) and focused instead on other unsteady effects.

Clap-and-fling

The clap-and-fling mechanism was first proposed by Weis-Fogh (1973) to explain the high lift generation in the chalcid wasp *Encarsia formosa* and is sometimes also referred to as the Weis-Fogh mechanism. A detailed theoretical analysis of the clap-and-fling can be found in Lighthill (1973) and Sunada et al. (1993), and experimental treatments in Bennett (1977), Maxworthy (1979) and Spedding and Maxworthy (1986).

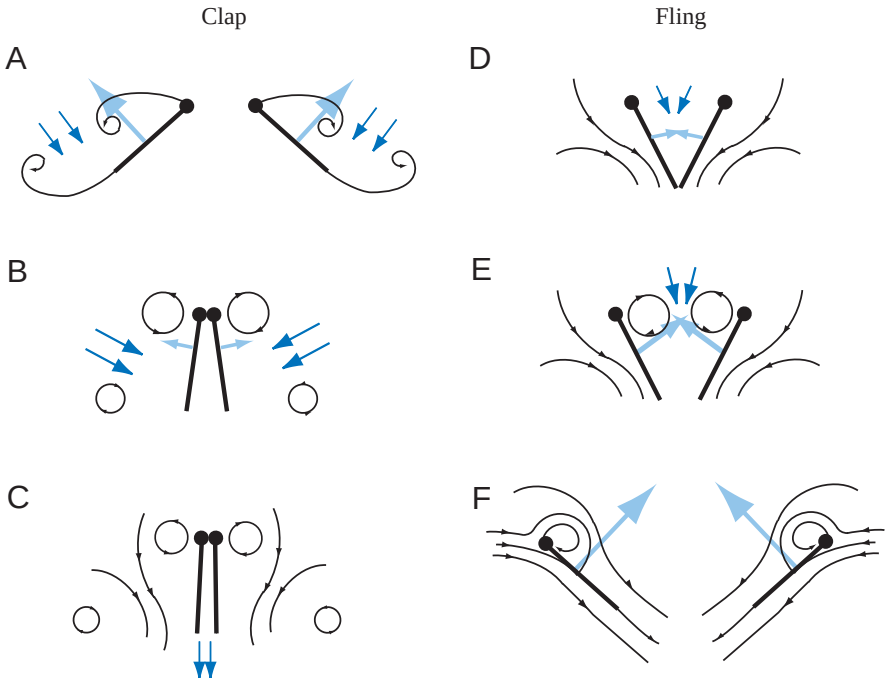

Fig. 4. Section schematic of wings approaching each other to clap (A–C) and flinging apart (D–F). Black lines show flow lines, and dark blue arrows show induced velocity. Light blue arrows show net forces acting on the airfoil. (A–C) Clap. As the wings approach each other dorsally (A), their leading edges touch initially (B) and the wing rotates around the leading edge. As the trailing edges approach each other, vorticity shed from the trailing edge rolls up in the form of stopping vortices (C), which dissipate into the wake. The leading edge vortices also lose strength. The closing gap between the two wings pushes fluid out, giving an additional thrust. (D–F) Fling. The wings fling apart by rotating around the trailing edge (D). The leading edge translates away and fluid rushes in to fill the gap between the two wing sections, giving an initial boost in circulation around the wing system (E). (F) A leading edge vortex forms anew but the trailing edge starting vortices are mutually annihilated as they are of opposite circulation. As originally described by Weis-Fogh (1973), this annihilation may allow circulation to build more rapidly by suppressing the Wagner effect.

Other variations of this basic mechanism, such as the clap-and-peel or the near-clap-and-fling, also appear in the literature (Ellington, 1984c). The clap-and-fling is really a combination of two separate aerodynamic mechanisms, which should be treated independently. In some insects, the wings touch dorsally before they pronate to start the downstroke. This phase of wing motion is called ‘clap’. A detailed analysis of these motions in *Encarsia formosa* reveals that, during the clap, the leading edges of the wings touch each other before the trailing edges, thus progressively closing the gap between them (Fig. 4A,B). As the wings press together closely, the opposing circulations of each of the airfoils annul each other (Fig. 4C). This ensures that the trailing edge vorticity shed by each wing on the following stroke is considerably attenuated or absent. Because the shed trailing edge vorticity delays the growth of circulation *via* the Wagner effect, Weis-Fogh (1973; see also Lighthill, 1973) argued that its absence or attenuation would allow the wings to build up circulation more rapidly and thus extend the benefit of lift over time in the subsequent stroke. In addition to the above effects, a jet of fluid excluded from the clapping wings can provide additional thrust to the insect (Fig. 4C; Ellington, 1984d; Ellington et al., 1996).

At the end of clap, the wings continue to pronate by leaving the trailing edge stationary as the leading edges ‘fling’ apart (Fig. 4D–F). This process generates a low-pressure region between them, and the surrounding fluid rushes in to occupy this region, providing an initial impetus to the build-up of circulation or attached vorticity (Fig. 4D,E). The two wings then translate away from each other with bound circulations of opposite signs. Although the attached circulation around each wing allows it to generate lift, the net circulation around the two-wing system is still zero and thus Kelvin’s law requiring conservation of circulation is satisfied (Fig. 4F; Spedding and Maxworthy, 1986). As pointed out by Lighthill (1973), this phenomenon is therefore also applicable to a fling occurring in a completely inviscid fluid. Collectively, the clap-and-fling could result in a modest, but significant, lift enhancement. However, in spite of its potential advantage, many insects never perform the clap (Marden, 1987). Others, such as *Drosophila melanogaster*, do clap under tethered conditions but only rarely do so in free flight. Because clap-and-fling is not ubiquitous among flying insects, it is unlikely to provide a general explanation for the high lift coefficients found in flying insects. Furthermore, when observed, the importance of the clap must always be weighed against a simpler alternative (but not mutually exclusive) hypothesis that the animal is simply attempting to maximize stroke amplitude, which can significantly enhance force generation. Several studies of peak performance suggest that peak lift production in both birds (Chai and Dudley, 1995) and insects (Lehmann and Dickinson, 1997) is constrained by the roughly 180° anatomical limit of stroke amplitude. Animals appear to increase lift by gradually expanding stroke angle until the wings either touch or reach some other morphological limit with the body. Thus, an insect exhibiting a clap may be attempting to maximize stroke amplitude. Furthermore, if it is indeed true that the Wagner effect only negligibly influences aerodynamic forces on insect wings, the classically described benefits of clap-and-fling may be less pronounced than previously thought. Resolution of these issues awaits a more detailed study of flows and forces during clap-and-fling.

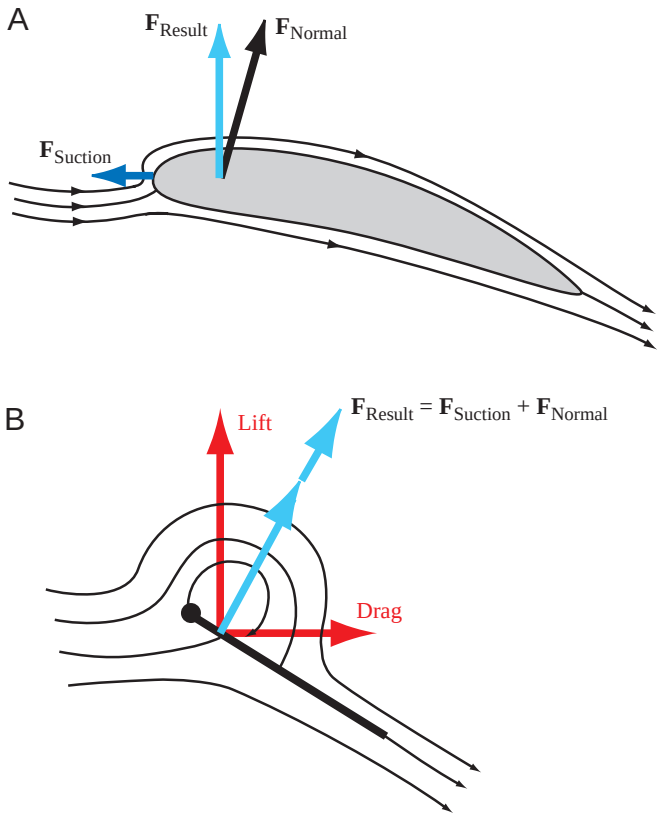

Fig. 5. Polhamus' leading edge suction analogy. (A) Flow around a blunt wing. The sharp diversion of flow around the leading edge results in a leading-edge suction force (dark blue arrow), causing the resultant force vector (light blue arrow) to tilt towards the leading edge and perpendicular to free stream. (B) Flow around a thin airfoil. The presence of a leading edge vortex causes a diversion of flow analogous to the flow around the blunt leading edge in A but in a direction normal to the surface of the airfoil. This results in an enhancement of the force normal to the wing section.

Delayed stall and the leading edge vortex

As the wing increases its angle of attack, the fluid stream going over the wing separates as it crosses the leading edge but reattaches before it reaches the trailing edge. In such cases, a leading edge vortex occupies the separation zone above the wing. Because the flow reattaches, the fluid continues to flow smoothly from the trailing edge and the Kutta condition is maintained. In this case, because the wing translates at a high angle of attack, a greater downward momentum is imparted to the fluid, resulting in substantial enhancement of lift. Experimental evidence and computational studies over the past 10 years have identified the leading edge vortex as the single most important feature of the flows created by insect wings and thus the forces they create.

Polhamus (1971) described a simple way to account for the enhancement of lift by a leading edge vortex that allows for an easy quantitative analysis. For blunt airfoils, air moves sharply around the leading edge, thus causing a leading edge suction force parallel to the wing chord. This extra force component adds to the potential force component (which acts normal to the wing plane), causing the resultant force to be perpendicular to the ambient flow velocity, i.e. in the direction of lift (Fig. 5A). At low angles of attack, this small forward rotation due to leading edge suction means that conventional airfoils better approximate the zero drag prediction of potential theory (Kuethe and Chow, 1998). However, for airfoils with sharper leading edge, flow separates at the leading edge, leading to the formation of a leading edge vortex. In this case, an analogous suction force develops not parallel but normal to the plane of the wing, thus adding to the potential force and consequently enhancing the lift component. Note that in this case, the resultant force is perpendicular to the plane of the wing and not to ambient velocity. Thus, drag is also increased (Fig. 5B).

For 2-D motion, if the wing continues to translate at high angles of attack, the leading edge vortex grows in size until flow reattachment is no longer possible. The Kutta condition breaks down as vorticity forms at the trailing edge creating a trailing edge vortex as the leading edge vortex sheds into the wake. At this point, the wing is not as effective at imparting a steady downward momentum to the fluid. As a result, there is a drop in lift, and the wing is said to have stalled. For several chord lengths prior to the stall, however, the presence of the attached leading edge vortex produces very high lift coefficients, a phenomenon termed 'delayed stall' (Fig. 6A). The first evidence for delayed stall in insect flight was by provided by Maxworthy (1979), who visualized the leading edge vortex on the model of a flinging wing. However, delayed stall was first identified experimentally on model aircraft wings as an augmentation in lift at the onset of motion at angles of attack above steady-state stall (Walker, 1931). At the lower Reynolds numbers appropriate for most insects, the breakdown of the Kutta condition is manifest by the growth of a trailing edge vortex, which then grows until it too can no longer stay attached to the wing (Dickinson and Götz, 1993). As the trailing edge vortex detaches and is shed into the wake, a new leading vortex forms. This dynamic process repeats, eventually creating a wake of regularly spaced counter-rotating vortices known as the 'von Karman vortex street' (Fig. 6A). The forces generated by the moving plate oscillate in accordance to the alternating pattern of vortex shedding. Although both lift and drag are greatest during phases when a leading edge vortex is present, forces are never as high as during the initial cycle.

The leading edge vortex may be especially important because insects flap their wings at high angles of attack. An experimental analysis of delayed stall in 2-D showed that flow separates to form a leading edge vortex at angles of attack above 9°, a threshold well below those used by insects (Dickinson and Götz, 1993). This study also directly measured time-variant force coefficients and showed that the values created by the presence of the leading edge vortex were at least sufficient to account for the 'missing force' in quasi-steady models. However, direct evidence that insect wings actually create leading edge vortices came from Ellington et

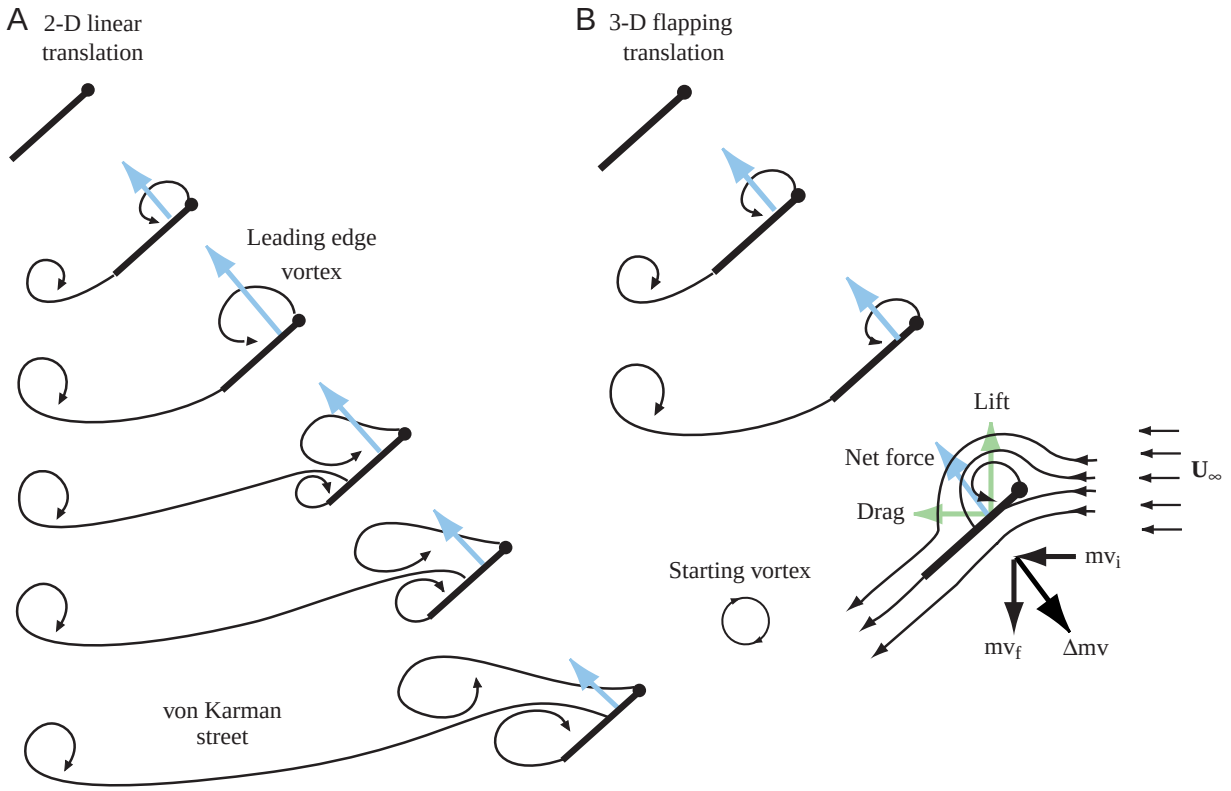

Fig. 6. A comparison of 2-D linear translation *vs* 3-D flapping translation. (A) 2-D linear translation. As an airfoil begins motion from rest, it generates a leading and trailing edge vortex. During translation, the trailing edge vortex is shed, leading to the growth of the leading edge vortex, which also sheds as the airfoil continues to translate. This motion leads to an alternate vortex shedding pattern from the leading and trailing edges, called the von Karman vortex street. This leads to a time dependence of the net aerodynamic forces (blue arrows) measured on the airfoil. (B) 3-D flapping translation. As in A, when an airfoil undergoing flapping translation starts from rest, it generates a leading and trailing edge vortex. However, as the motion progresses, the leading edge vortex attains a constant size and does not grow any further. Because no new vorticity is generated at the leading edge, there is no additional vorticity generated at the trailing edge and the airfoil obeys the Kutta condition. When established, the Kutta condition ensures that there is a net change in the direction of momentum resulting in a reactive aerodynamic force on the airfoil (black arrows; mv_i signifies initial momentum, mv_f signifies final momentum and Δmv signifies the difference between initial and final momenta). After establishment of the Kutta condition, the measured net aerodynamic forces (blue arrows) stay stable over a substantial period during translation and do not show time dependence. For Reynolds numbers of ≥100, this force acts normally to the wing and can be decomposed into mutually orthogonal lift and drag components (green arrows). Ultimately, however, the net downward momentum imparted by the airfoil to the fluid causes a downwash that slightly lowers the constant value of the net aerodynamic force on a steadily revolving wing.

al. (1996), who used smoke to visualize the flow around both real and 3-D model *Manduca sexta* at a Reynolds number in the range of 10^3. In contrast to 2-D models, the leading edge vortex was not shed even after many chords of travel and thus never created a pattern analogous to a von Karman street. Thus, the wing never stalls under these conditions (Fig. 6B). These observations have been confirmed at lower Reynolds numbers in experiments on model fruit fly wings, which showed that forces, like flows, are remarkably stable during constant flapping (Dickinson et al., 1999). What causes this prolonged attachment of the leading edge vortex on a flapping wing compared to the 2-D case? In their model hawkmoth, Ellington and co-workers observed a steady span-wise flow from the wing hinge to approximately three-quarters of the distance to the wing tip, at which point the leading edge vortex detaches from the wing surface. This spanwise flow is entrained by the leading edge vortex, causing it to spiral towards the tip of the wing (Fig. 7). A similar flow was observed by Maxworthy (1979) during early analysis of the 3-D fling. Because this flow redirects momentum transfer in the spanwise direction, it should correspondingly reduce the momentum of the flow from the chordwise direction, causing the leading edge vortex to remain smaller. A smaller leading edge vortex allows the fluid to reattach more easily and the wing can sustain this reattachment for a longer time. Thus, axial flow appears to serve a useful role by maintaining stable attachment of the leading edge vortex. As pointed out by Ellington, a similar leading edge vortex is stabilized by an axial flow generated due to the back-sweep of wings in delta aircraft such as the Concorde, creating one of the more

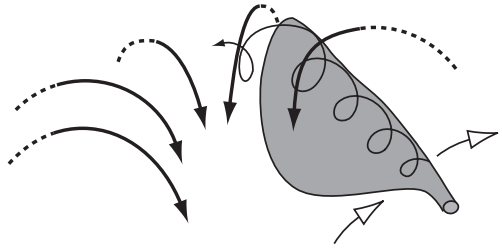

Fig. 7. Stable attachment of the leading edge vortex. As the flapping wing translates, a span-wise velocity gradient interacts with the leading edge vortex, causing the axial flow to spiral towards the tip. The axial flow transports momentum out of the vortex, thus keeping it stably attached. The vortex detaches at about three-quarters of the distance to the wing tip and is shed into the wake. Thick black arrows indicate downwash due to the vortex system generated by the wing in its surrounding fluid. Figure adapted from VandenBerg and Ellington (1997).

remarkable analogies between the biological and mechanized worlds.

Recently, using DPIV to map the flow structure on a model fruit fly wing (*Re*=115), Birch and Dickinson (2001) reported stable attachment of the leading edge vortex in the absence of a prominent helical vortex. Whereas the axial flow within the core of the vortex was nearly an order of magnitude lower than on the *Manduca* model in *Re*=10^3 range, they observed a prominent axial flow within a broad sheet of fluid on top of the wing behind the leading edge vortex that rolls into a prominent tip vortex. These results from model hawkmoths and fruit flies suggest that the 3-D flow structure may be quantitatively different at high and low Reynolds numbers.

Interestingly, the observed differences in the 3-D flow structures do not seem to be reflected in the measured forces. CFD simulations in 2-D (Wang, 2000; Hamdani and Sun, 2000) and 3-D (Ramamurti and Sandberg, 2002) airfoils show a remarkable similarity in forces calculated at *Re*=100 and those calculated using the inviscid Euler equation corresponding to an infinite *Re* (or *Re*=100 000 in the case of Hamdani and Sun, 2000). These results suggest that although viscosity is necessary for vorticity generation, its contribution to net forces is very small beyond *Re*=100 and the forces may be predominantly due to the dynamic pressure gradients across the wing. The above conclusions from CFD models are also supported by empirical data (Usherwood and Ellington, 2002b). Together, these results present a somewhat paradoxical conclusion that forces remain relatively unaffected even when flow structures vary substantially with an increase in Reynolds number above 100.

Although a detailed explanation of above results awaits a more rigorous quantification of simultaneous flow and force data, these differences should not obscure the more salient general features of separated flow at high angles of attack. In particular, the absence of periodic shedding in these recent experiments indicates that the 3-D flow around a flapping wing may be remarkably self-stabilizing over a Reynolds number range of ≥100. For the existence of such stability, the creation of vorticity at the leading edge is matched perfectly by the convection and diffusion of vorticity into the wake, thus creating a stable equilibrium. This situation may be analogous to the continuous attachment of vortices behind bluff bodies at Reynolds numbers below the threshold for von Karman shedding (see, for example, Acheson, 1990). What maintains the balance in creation and transport of vorticity and how does this change with Reynolds number? Similarly, what determines the magnitude of the leading edge vortex supported by a flapping wing at equilibrium? Given the importance of the leading edge vortex, the answers to these questions are critical to determining the limits of aerodynamic performance in insect flight.

Kramer effect (rotational forces)

Near the end of every stroke, insect wings undergo substantial pronation and supination about a spanwise axis, which allows them to maintain a positive angle of attack and generate lift during both forward and reverse strokes. Furthermore, there is some evidence from both tethered (Dickinson et al., 1993) and free (Srygley and Thomas, 2002) flight that insects alter the timing of rotation during flight maneuvers. The aerodynamic significance of these rotations for flapping flight has been studied by Bennett (1970), and more recently in detail by Sane and Dickinson (2002), but it is well known in the aerodynamic literature in the context of fluttering airplane wings due to the extensive theoretical work of Munk (1925b), Glauert (1929), Theodorsen (1935), Fung (1969) and supporting experimental evidence from Kramer (1932), Reid (1927), Farren (1935), Garrick (1937), Silverstein and Joyner (1939) and Halfman (1951).

When a flapping wing rotates about a span-wise axis while at the same time translating, flow around the wing deviates from the Kutta condition and the stagnation region moves away from the trailing edge. This causes a sharp, dynamic gradient at the trailing edge, leading to shear. Because fluids tend to resist shear due to their viscosity, additional circulation must be generated around the wing to re-establish the Kutta condition at the trailing edge. In other words, the wing generates a rotational circulation in the fluid to counteract the effects of rotation. The re-establishment of Kutta condition is not instantaneous, however, but requires a finite amount of time. If, in this time, the wing continues to rotate rapidly, then the Kutta condition may never be actually observed at any given instant of time during the rotation but the tendency of the fluid towards its establishment may nevertheless dictate the generation of circulation. Thus, extra circulation proportional to the angular velocity of rotation continues to be generated until smooth, tangential flow can be established at the trailing edge. Depending on the direction of rotation, this additional circulation causes rotational forces that either add to or subtract from the net force due to translation. This effect is also often called the ‘Kramer effect’, after M. Kramer who first described it (Kramer, 1932), or alternatively as ‘rotational forces’ (Sane and Dickinson, 2002).

Using the conceptual framework described above, Sane and Dickinson (2002) measured rotational coefficients (Kramer effect) and, following the recommendation of Ellington (1984d,f), included them with the translational coefficients in the existing quasi-steady models. The revised quasi-steady model was able to capture the corresponding time history of the force traces, in addition to the stroke-averaged forces, better than the quasi-steady models that take only translation into account. Similar rotational force peaks were observed in CFD simulations by Sun and Tang (2002), who described these peaks as arising from 'fast pitching-up rotation of the wing near the end of the stroke', but appear essentially complementary to the Kramer effect. Both the revised quasi-steady model and CFD models show close agreement with the experimental measurements.

It is important to note that the Kramer effect (or the rotational force of Sane and Dickinson, 2002) is fundamentally different from the Magnus force, to which a loose qualitative analogy was drawn in the past literature (Bennett, 1970; Dickinson et al., 1999), leading to some confusion. Magnus force arises from circulation generated by a blunt body such as a spinning cylinder or sphere set into translational motion with respect to the real fluid (see, for example, Prandtl and Tietjens, 1957a). Although the Magnus force can be calculated from this circulation using Kutta–Jukowski theorem (as in airfoils), it excludes either explicit or implicit application of the Kutta condition because, by definition, blunt bodies have no surface singularities where such a condition can hold. On the other hand, the application of the Kutta condition is necessary and fundamental to all calculations of aerodynamic forces on thin airfoils. As a result, the mechanism of Magnus force applies only in relation to cylinders, spheres and blunt objects, and extending it to complex surfaces such as thin airfoils or other surfaces with sharp edges is, at best, problematic (Schlichting, 1979). Not surprisingly, therefore, the Magnus effect does not provide an explanation of the rotational forces during pronation or supination (Sun and Tang, 2002), nor is it possible to apply it to calculations of forces or circulation on a flapping thin airfoil without making severe assumptions (Walker, 2002).

Added mass

All the forces described in the previous section belong to the class of circulatory forces because their action can be mathematically described by calculating the changes in the velocity potential around the wing. As previously described, an inclined wing moving at a constant angle of attack is subject to aerodynamic forces that can be adequately modeled by accounting for the circulation around the wing using standard potential theory. Other effects such as leading edge separation may also be modeled by a variation of the same approach (see, for example, Minotti, 2002). However, when the wing accelerates, it encounters a reaction force due to the accelerated fluid. This reactive non-circulatory force (Sedov, 1965) falls outside the realm of standard circulation-based steady-state analyses and is variably called 'added mass' (Vogel, 1994), 'added mass inertia' (Sane and Dickinson, 2001), 'acceleration reaction' (Daniel, 1984; Denny, 1993) or 'virtual mass' (Ellington, 1984b) within the biological literature. Because these forces typically occur at the same time as the circulatory forces, it is usually difficult to measure them in isolation. In addition, they also pose some difficulty in modeling because added mass inertia has components arising from acceleration of fluid relative to the wing, rotational acceleration due to wing rotation and a cross-term arising from translational velocity and angular velocity (Ellington, 1984d). It is possible, however, to estimate the magnitude of added mass relative to the contribution of circulatory forces.

Methods of calculating added mass have been outlined in various texts, most notably in Sedov (1965), Denny (1993) and Lighthill (1975) or in research articles by Ellington (1984d), Sunada et al. (2001), Sane and Dickinson (2002), Zbikowski (2002) and Minotti (2002). The added mass force is typically modeled in quasi-steady terms using a time-invariant added-mass coefficient, and any time dependence is implicit due to the time course of wing acceleration. In a computational study of a 2-D insect wing, Hamdani and Sun (2000) simulated a series of impulsive starts at different accelerations. Their force predictions, based on the time derivative of the moment of vorticity integral (equation 11) over their simulated flow field, accurately matched prior experimental results. The acceleratory forces at the start of translation corresponded to a rapid rise in the moment of vorticity. At this early stage of motion, the rise in the moment of vorticity is due to both the convection and growth of vorticity. Thus, added mass forces are closely tied to the initial stages of flow separation and fluid acceleration, and further experimental investigations offer a promising area for further research.

Wing–wake interactions

The reciprocating pattern of wing motion used by insects suggests that their wings might potentially interact with the shed vorticity of prior strokes. That such interactions can result in significant forces was first observed during 2-D motion on an inclined plate (Dickinson, 1994). A similar phenomenon was also observed with both force measurements and flow visualization on a 3-D mechanical model of a fruit fly (Dickinson et al., 1999). As the wing reverses stroke (Fig. 8A–C), it sheds both the leading and the trailing edge vortices (Fig. 8C). These shed vortices induce a strong inter-vortex velocity field, the magnitude and orientation of which are governed by the strength and position of the two vortices (Fig. 8C,D). As the wing reverses direction, it encounters the enhanced velocity and acceleration fields, thus resulting in higher aerodynamic forces immediately following stroke reversal (Fig. 8E). This phenomenon has been alternatively called 'wake capture' or, more accurately, wing–wake interaction. The magnitude and relative strengths of the shed vortices, and therefore wake capture, are strongly dependent

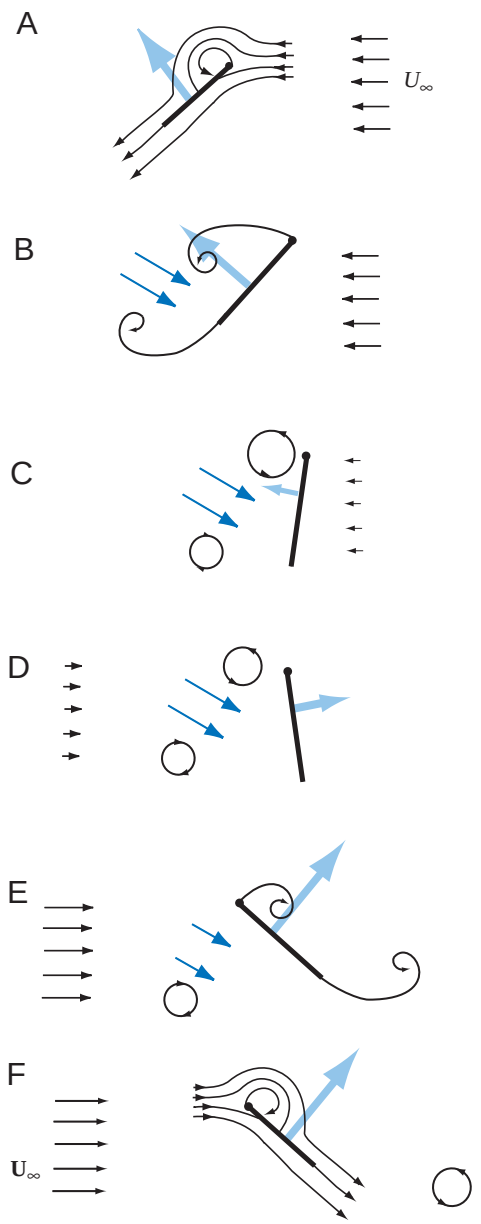

Fig. 8 A hypothesis for wing–wake interactions. Parts A–F depict a wing section as it reverses stroke. As the wing transitions from a steady translation (A) phase and rotates around a chordwise axis in preparation for a stroke reversal, it generates vorticity at both the leading and trailing edges (B). These vortices induce a strong velocity field (dark blue arrows) in the intervening region (C,D). As the wing comes to a halt and then reverses stroke (D,E), it encounters this jet. As the wing interacts with its wake, a peak is registered in the aerodynamic force record (light blue arrows), which is sometimes called wake capture or wing–wake interaction. U_∞, free-stream velocity.

on the kinematics of the wing immediately before and after stroke reversal.

Recently, Sun and Tang (2002) performed CFD simulations for the kinematics similar to those in Dickinson et al. (1999) and have proposed that the initial force peak is due to acceleration of the wing rather than due to wing–wake interactions. To show that wing–wake interaction produces a negligible effect on forces, they started a wing from rest (in still air) and compared the calculated forces with the forces on a wing undergoing identical motion after stroke reversal. Interestingly, the forces were nearly identical in the two cases and they did not observe any force peaks due to wing–wake interactions. Second, they varied the period of acceleration of the wing immediately after stroke reversal. For higher values of acceleration, they calculated force peaks similar in magnitude and dynamics to the experiments of Dickinson et al. (1999). From these experiments, they concluded that the forces related to the acceleration of the wing, not wing–wake interactions, fully account for the force peaks immediately following stroke reversal.

These results are puzzling for two reasons. First, to verify their hypothesis of wing–wake interactions, Dickinson et al. (1999) stopped the wing at stroke reversal. They argued that if forces were augmented due to relative velocity between the wing and the induced wake, then even a non-accelerating wing should continue to generate forces as it encounters the wake from its previous stroke. The results of these experiments (fig. 4 of Dickinson et al., 1999), strongly suggested that wing–wake interactions can indeed contribute significantly to the aerodynamic forces immediately after stroke reversal. Second, they visualized the near-field wake structure at the instant of stroke reversal using particle image velocimetry. These images revealed the substantial wake induced by the previous stroke and also demonstrated its physical interaction with the wing in the period immediately following stroke reversal (Fig. 8A–E). It seems unlikely that this wing–wake interaction would not be reflected in the time history of the corresponding aerodynamic forces. At present, the cause of this discrepancy between the CFD simulations (Sun and Tang, 2002) and the particle image velocimetric observations (Dickinson et al., 1999) remains unclear. In any case, these results strongly suggest that neither the wing acceleration nor the wing–wake interactions should be ignored when modeling wake capture.

Current status of quasi-steady modeling

Many of the mechanisms outlined above may be described by simple algebraic equations provided steady-state assumption holds true. Because it is difficult to solve for the full Navier–Stokes equations for flows around insect wings, equations based on quasi-steady assumptions still hold some practical utility in a comprehensive model of insect flight. The lift and drag coefficients for flapping 3-D motions were investigated first by Jensen (1956), Vogel (1967), Rees (1975), Dudley and Ellington (1990a,b), Willmott and Ellington (1997a) and Nachtigall (1977) on actual insects wings and more recently on the physical models of flapping insect wings by Dickinson et al. (1999), Sane and Dickinson (2001) and Usherwood and Ellington (2002a,b) and in the computational fluid dynamic models by Sun and Tang (2002).

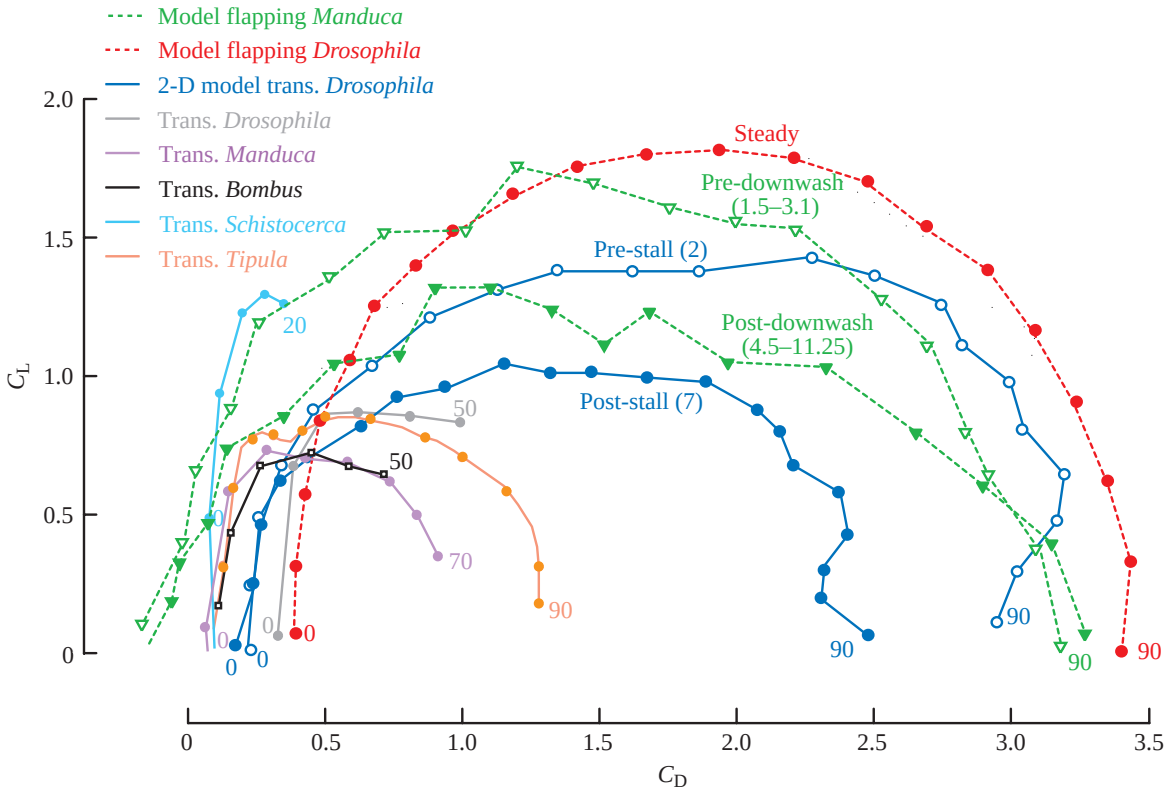

Fig. 9. Polar plot comparisons of data from different studies of insect flight. Dotted lines signify coefficients for flapping translation and continuous lines for non-flapping translation. The values in parentheses signify the upper and lower limits of travel in chord lengths within which values were averaged. Values at the beginning and end of each plot signify the angle of attack in degrees. These data are derived from the following studies: *Tipula oleracea* (*Re*=1500; orange; Nachtigall, 1977), *Schistocerca gregaria* (*Re*=2000; light blue; Jensen, 1956), *Bombus* (*Re*=2500; black; Dudley and Ellington, 1990b), *Manduca sexta* (*Re*=7300; purple; Willmott and Ellington, 1997a), *Drosophila virilis* (*Re*=200; grey; Vogel, 1967), 2-D model *Drosophila* wings (*Re*=200; dark blue; Dickinson and Götz, 1993), model flapping *Drosophila* (*Re*=150; red; Dickinson et al., 1999), model flapping *Manduca* (*Re*=8000; green; Usherwood and Ellington, 2002a). Please note that the Reynolds number (*Re*) values are approximate and broadly representative of the aerodynamic regime. C_D, coefficient of drag; C_L, coefficient of lift.

Fig. 9 shows a comparison among the lift-drag polars during steady translation in non-flapping finite and infinite wings, as well as for flapping wings. The aerodynamic coefficients measured on flapping wings are significantly higher than the corresponding coefficients for non-flapping finite wings. There are several explanations for the significant differences. First, the data on non-flapping finite wings represent time-averaged forces collected on finite wings placed at fixed angles of attack in a wind tunnel. If the non-flapping finite wings exhibited von Karman vortex shedding, the force records would fail to reflect the benefits of an initial temporary attachment of the leading edge vortex, thus causing the force coefficients on flapping wings to be higher than the force coefficients for non-flapping finite wings. Moreover, the steady coefficients measured on flapping wings are similar in magnitude to the ‘early’, pre-stall force coefficients (measured at two chord length motion and before von Karman shedding occurs) on an impulsively started 2-D plate whereas the non-flapping finite wings are similar in magnitude to the ‘late’, post-stall force coefficients of the same profiles (Dickinson and Götz, 1993). The instantaneous forces measured on a flapping wing at constant angles of attack provide further evidence that flapping wings do not show von Karman shedding. In addition, following the inertial transients arising from the impulsive start of the airfoil, the instantaneous force coefficients reach steady values that remain constant through a substantial duration of flapping translation (Dickinson et al., 1999). However, if the wing continues the flapping translation, the wings eventually show some decline in performance. This may be explained by the fact that a wing revolving in a propeller-like fashion eventually establishes a strong downwash in the far-field, thus lowering the effective angles of attack (Usherwood and Ellington, 2002a). An alternative view is that, under steady flow conditions, non-flapping finite wings with aspect ratios typical of insect wings do not exhibit vortex shedding. Like flapping wings, they rapidly attain a stable pattern of flow – although the strength of the total circulation is substantially lower than with a flapping motion at comparable angles of attack. In this view, there is some feature of flapping motion – such as the span-wise gradient in chord-wise velocity – that allows the leading edge vortex to attain a greater strength than in the non-flapping case. In the future, these issues might be resolved by

simultaneous flow visualization and force measurement under the two experimental conditions. Of special interest are differences in convective processes such as axial flow (Ellington et al., 1996), downwash induced by tip vortices or diffusion that might limit the growth of vorticity at the leading edge to different degrees in the two cases.

When we revisit the proof-by-contradiction method using these higher values of steady lift and drag coefficients appearing in the recent literature on flapping wings, the calculated average forces are proportionally higher and sufficient to explain hovering. This has led to a revival of the quasi-steady models in recent years. Indeed, when rotational coefficients are included along with the translational coefficients in the quasi-steady model, the time course of aerodynamic force generation is also well captured (Sane and Dickinson, 2002). However, such a model cannot yet account for the force peaks resulting from wing–wake interactions.

Future research and directions

Because both the absence of stall and Kramer effect can be modeled using potential flow theory, the above results suggest that simple analytical models can satisfactorily describe the aerodynamic forces due to translation and rotation in a flapping wing. It is also necessary to incorporate the unsteady components due to wing–wake interactions and the non-circulatory forces due to added mass into such models. Finally, it is necessary to account for wing flexibility since the above models are based on rigid wings. In general, the problem of wing flexibility is very complex due to the various aero-elastic effects on a moving wing. However, recent studies on wing flexibility indicate that most of the wing flexion occurs not from the aero-elastic interactions between the wing and the fluid but simply from the inertial bending of the wing on account of its mass distribution (Daniel and Combes, 2002). These results promise to substantially simplify the incorporation of wing flexion into current quasi-steady models.

These developments in the area of insect flight aerodynamics will prove critical to biologists who seek to understand how flight and flight-related adaptations have enabled insects to be so extraordinarily successful in the course of their evolution. In addition, they also promise to be useful in breaking new ground in technology. The recent interest in developing insect-inspired micro air vehicles (MAVs; also called micro-mechanical flying insects or MFIs) has fostered a number of strong collaborations between analytical and computational fluid dynamicists, micro-robotics engineers and insect flight biologists (Ellington, 1999; Zbikowski, 2002). The combination of expertise from these different areas promises to help insect flight biologists ask questions and devise experiments that were previously inconceivable. From an academic standpoint, the success of these projects will allow us to satisfactorily demonstrate our understanding of the fundamental fluid dynamic mechanisms underlying insect flight.

List of symbols

$\hat{\nabla}$	del operator
A	cross-sectional area of wing
C_D	drag coefficient
C_L	lift coefficient
$d\hat{\mathbf{l}}$	non-dimensional length element along the contour and tangential at each point on it
$\mathbf{i}$	unit Cartesian vector
$\mathbf{j}$	unit Cartesian vector
$\mathbf{k}$	unit Cartesian vector
L	length
$\hat{L}'$	non-dimensional lift per unit span
$\hat{\mathbf{n}}d\hat{S}$	non-dimensional area surface element directed normal to the surface
$\hat{P}$	non-dimensional pressure
R	area of region of interest encompassing all vorticity elements
$\mathbf{r}$	displacement vector or distance vector
r	distance
Re	Reynolds number
$\hat{t}$	non-dimensional time
U_∞	free-stream velocity
$\hat{\mathbf{u}}$	non-dimensional velocity of the flapping wing
U'	downwash velocity
$\mathbf{v}$	velocity
V	volume
Φ	scalar potential function
Γ	circulation
Σ	contour around the wing section
α	geometric angle of attack
α'	aerodynamic or effective angle of attack
γ	first moment of vorticity
η	dynamic viscosity of fluid
ρ	density of fluid
$\boldsymbol{\omega}$	vorticity of fluid
$\hat{\boldsymbol{\omega}}$	non-dimensional vorticity of fluid

I am deeply indebted to Michael Dickinson for his generous input and encouragement during the writing of this manuscript; Tom Daniel and Charlie Ellington for their support and critical comments; and Kathryn Phillips for comments on an early draft. Thanks to two anonymous reviewers for their critical input, which greatly improved the manuscript. Support was provided by an Office of Naval Research MURI grant to Tom Daniel.

References

Acheson, D. (1990). Elementary fluid dynamics. In *Oxford Applied Mathematics and Computing Science series* (ed. R. Churchouse, W. McColl and A. Tayler), pp. 157-200. Oxford: Oxford University Press.

Azuma, A., Azuma, S., Watanabe, I. and Furuta, T. (1985). Flight mechanics of a dragonfly. *J. Exp. Biol.* **116**, 79-107.

Azuma, A. and Watanabe, T. (1988). Flight performance of a dragonfly. *J. Exp. Biol.* **137**, 221-252.

Batchelor, G. K. (1973). *An Introduction to Fluid Dynamics*. Cambridge, New York: Cambridge University Press.

Bennett, L. (1970). Insect flight: lift and the rate of change of incidence. *Science* **167**, 177-179.

Bennett, L. (1977). Clap and fling aerodynamics – an experimental evaluation. *J. Exp. Biol.* **69**, 261-272.
Birch, J. and Dickinson, M. H. (2001). Spanwise flow and the attachment of the leading-edge vortex. *Nature* **412**, 729-733.
Brodsky, A. K. (1994). *The Evolution of Insect Flight*. New York: Oxford University Press.
Buckholz, R. H. (1981). Measurements of unsteady periodic forces generated by the blowfly flying in a wind tunnel. *J. Exp. Biol.* **90**, 163-173.
Chai, P. and Dudley, R. (1995). Maximum right performance and limits to power output of vertebrate striated-muscle. *FASEB J.* **9**, A353.
Cloupeau, M., Devillers, J. F. and Devezeaux, D. (1979). Direct measurements of instantaneous lift in desert locust; comparison with Jensen's experiments on detached wings. *J. Exp. Biol.* **80**, 1-15.
Daniel, T. (1984). Unsteady aspects of aquatic locomotion. *Am. Zool.* **24**, 121-134.
Daniel, T. and Combes, S. (2002). Flexing wings and fins: bending by inertial or fluid dynamic forces? *Int. Comp. Biol.* **42**, 1044-1049.
Denny, M. (1993). *Air and Water: The Biology and Physics of Life's Media*. Princeton, NJ: Princeton University Press.
Dickinson, M. H. (1994). The effects of wing rotation on unsteady aerodynamic performance at low Reynolds numbers. *J. Exp. Biol.* **192**, 179-206.
Dickinson, M. H. and Götz, K. G. (1993). Unsteady aerodynamic performance of model wings at low Reynolds numbers. *J. Exp. Biol.* **174**, 45-64.
Dickinson, M. H., Lehmann, F.-O. and Götz, K. G. (1993). The active control of wing rotation by *Drosophila*. *J. Exp. Biol.* **182**, 173-189.
Dickinson, M. H., Lehmann, F.-O. and Sane, S. P. (1999). Wing rotation and the aerodynamic basis of insect flight. *Science* **284**, 1954-1960.
Dudley, R. (1991). Biomechanics of flight in neotropical butterflies – aerodynamics and mechanical power requirements. *J. Exp. Biol.* **159**, 335-357.
Dudley, R. (2000). *The Biomechanics of Insect Flight*. Princeton, NJ: Princeton University Press.
Dudley, R. and Ellington, C. P. (1990a). Mechanics of forward flight in bumblebees. 1. Kinematics and morphology. *J. Exp. Biol.* **148**, 19-52.
Dudley, R. and Ellington, C. P. (1990b). Mechanics of forward flight in bumblebees. 2. Quasi-steady lift and power requirements. *J. Exp. Biol.* **148**, 53-88.
Ellington, C. P. (1978). The aerodynamics of normal hovering flight: three approaches. In *Comparative Physiology: Water, Ions and Fluid mechanics* (ed. K. Schmidt- Nielsen, L. Bolis and S. Maddrell), pp. 327-345. Cambridge: Cambridge University Press.
Ellington, C. P. (1980). Vortices and hovering flight. In *Instationare Effekte an schwingended Fluegeln* (ed. W. Nachtigall), pp. 64-101. Weisbaden: F. Steiner.
Ellington, C. P. (1984a). The aerodynamics of hovering insect flight. I. The quasi-steady analysis. *Phil. Trans. R. Soc. Lond. B* **305**, 1-15.
Ellington, C. P. (1984b). The aerodynamics of hovering insect flight. II. Morphological parameters. *Phil. Trans. R. Soc. Lond. B* **305**, 17-40.
Ellington, C. P. (1984c). The aerodynamics of hovering insect flight. III. Kinematics. *Phil. Trans. R. Soc. Lond. B* **305**, 41-78.
Ellington, C. P. (1984d). The aerodynamics of hovering insect flight. IV. Aerodynamic mechanisms. *Phil. Trans. R. Soc. Lond. B* **305**, 79-113.
Ellington, C. P. (1984e). The aerodynamics of hovering insect flight. V. A vortex theory. *Phil. Trans. R. Soc. Lond. B* **305**, 115-144.
Ellington, C. P. (1984f). The aerodynamics of hovering insect flight. VI. Lift and power requirements. *Phil. Trans. R. Soc. Lond. B* **305**, 145-181.
Ellington, C. P. (1999). The novel aerodynamics of insect flight: applications to micro- air vehicles. *J. Exp. Biol.* **202**, 3439-3448.
Ellington, C. P., Van den Berg, C., Willmott, A. P. and Thomas, A. L. R. (1996). Leading-edge vortices in insect flight. *Nature* **384**, 626-630.
Ennos, A. R. (1989a). Inertial and aerodynamic torques on the wings of Diptera in flight. *J. Exp. Biol.* **142**, 87-95.
Ennos, A. R. (1989b). The kinematics and aerodynamics of the free flight of some Diptera. *J. Exp. Biol.* **142**, 49-85.
Farren, W. S. (1935). The reaction on a wing whose angle of incidence is changing rapidly. *Rep. Memo. Aeronaut. Res. Comm. (Great Britain) 1648*.
Fung, Y. C. (1969). *An Introduction to the Theory of Aeroelasticity*. New York: Dover.
Garrick, I. E. (1937). Propulsion of a flapping and oscillating airfoil. *NACA report* **567**, 419-427.
Glauert, H. (1929). The force and moment on an oscillating airfoil. *Rep. Memo. Aeronaut. Res. Comm. (Great Britain) no. 1561*.
Glauert, H. (1947). *The Elements of Aerofoil and Airscrew Theory*. New York: Cambridge Science Classics.
Halfman, R. (1951). Experimental aerodynamic derivatives of a sinusoidally oscillating airfoil in two-dimensional flow. *NACA TN 2465*.
Hamdani, H. and Sun, M. (2000). Aerodynamic forces and flow structures of an airfoil in some unsteady motions at small Reynolds number. *Acta Mechanica* **145**, 173-187.
Hamdani, H. and Sun, M. (2001). A study on the mechanism of high-lift generation by an airfoil in unsteady motion at low Reynolds number. *Acta Mechanica Sinica* **17**, 97-114.
Jensen, M. (1956). Biology and physics of locust flight. III The aerodynamics of locust flight. *Phil. Trans. R. Soc. Lond. B* **239**, 511-552.
Kramer, M. (1932). Die Zunahme des Maximalauftriebes von Tragflugeln bei plotzlicher Anstellwinkelvergrosserung (Boeneffekt). *Z. Flugtech. Motorluftschiff.* **23**, 185-189.
Kuethe, A. and Chow, C.-Y. (1998). *Foundations of Aerodynamics: Bases of Aerodynamic Design*. New York: John Wiley & Sons.
Lamb, H. (1945). *Hydrodynamics*. New York: Dover Publications.
Landau, L. D. and Lifshitz, E. M. (1959). *Fluid Mechanics*. London: Pergamon Press.
Lehmann, F.-O. and Dickinson, M. H. (1997). The changes in power requirements and muscle efficiency during elevated force production in the fruit fly *Drosophila melanogaster*. *J. Exp. Biol.* **200**, 1133-1143.
Lighthill, M. (1973). On Weis-Fogh mechanism of lift generation. *J. Fluid Mech.* **60**, 1-17.
Lighthill, M. (1975). Mathematical biofluiddynamics. In *Regional Conference Series in Applied Mathematics*, vol. 17. Philadelphia: Society for Industrial and Applied Mathematics.
Liu, H., Ellington, C. P., Kawachi, K., Van den Berg, C. and Willmott, A. P. (1998). A computational fluid dynamic study of hawkmoth hovering. *J. Exp. Biol.* **201**, 461-477.
Liu, H. and Kawachi, K. (1998). A numerical study of insect flight. *J. Comput. Physics* **146**, 124-156.
Marden, J. H. (1987). Maximum lift production during takeoff in flying animals. *J. Exp. Biol.* **130**, 235-258.
Maxworthy, T. (1979). Experiments on the Weis-Fogh mechanism of lift generation by insects in hovering flight. Part 1. Dynamics of the 'fling'. *J. Fluid Mech.* **93**, 47-63.
Milne-Thomson, L. M. (1966). *Theoretical Aerodynamics*. London, New York: Macmillan, St Martin's Press.
Minotti, F. (2002). Unsteady two-dimensional theory of a flapping wing. *Phys. Rev. E* **66**, art. no. 051907.
Munk, M. (1925a). Elements of the wing section theory and of wing theory. *NACA Report* **191**, 141-163.
Munk, M. (1925b). Note on the air forces on a wing caused by pitching. *NACA TN 217*.
Nachtigall, W. (1977). Die Aerodynamische Polare des Tipula-Flugels und eine Einrichtung zur halbautomatischen Polarenaufnahme. In *The Physiology of Movement: Biomechanics* (ed. W. Nachtigall), pp. 347-352. Stuttgart: Fischer.
Norberg, R. (1975). Hovering flight of the dragonfly, *Aeschna juncea* L., kinematics and aerodynamics. In *Swimming and Flying in Nature*, vol. 2 (ed. T. Wu, C. Brokaw and C. Brennen), pp. 763-781. New York: Plenum Press.
Osborne, M. F. M. (1950). Aerodynamics of flapping flight with application to insects. *J. Exp. Biol.* **28**, 221-245.
Polhamus, E. (1971). Predictions of vortex-lift characteristics by a leading-edge suction analogy. *J. Aircraft* **8**, 193-199.
Prandtl, L. and Tietjens, O. K. G. (1957a). *Applied Hydro- and Aeromechanics; Based on Lectures of L. Prandtl*. New York: Dover Publications.
Prandtl, L. and Tietjens, O. K. G. (1957b). *Fundamentals of Hydro- and Aeromechanics*. New York: Dover Publications.
Ramamurti, R. and Sandberg, W. C. (2002). A three-dimensional computational study of the aerodynamic mechanisms of insect flight. *J. Exp. Biol.* **205**, 1507-1518.
Rayner, J. M. V. (1979a). A vortex theory of animal flight. Part 1. The vortex wake of a hovering animal. *J. Fluid Mech.* **91**, 697-730.
Rayner, J. M. V. (1979b). A vortex theory of animal flight. Part 2. The forward flight of birds. *J. Fluid Mech.* **91**, 731-763.
Rees, C. (1975). Aerodynamic properties of an insect wing section and a smooth aerofoil compared. *Nature* **258**, 141-142.
Reid, E. (1927). Airfoil lift with changing angle of attack. *NACA TN 266*.
Ruppell, G. (1989). Kinematic analysis of symmetrical flight manoeuvres of odonata. *J. Exp. Biol.* **144**, 13-43.

Sane, S. P. and Dickinson, M. H. (2001). The control of flight force by a flapping wing: lift and drag production. *J. Exp. Biol.* **204**, 2607-2626.
Sane, S. P. and Dickinson, M. H. (2002). The aerodynamic effects of wing rotation and a revised quasi-steady model of flapping flight. *J. Exp. Biol.* **205**, 1087-1096.
Sato, M. and Azuma, A. (1997). Flight performance of a damselfly *Ceriagrion melanurum* Selys. *J. Exp. Biol.* **200**, 1765-1779.
Savage, S., Newman, B. and Wong, D. (1979). The role of vortices and unsteady effects during the hovering flight of dragonflies. *J. Exp. Biol.* **83**, 59-77.
Schlichting, H. (1979). *Boundary-Layer Theory*. New York: McGraw-Hill.
Sedov, L. I. (1965). *Two-Dimensional Problems in Hydrodynamics and Aerodynamics* (ed. C. Chu, H. Cohen and B. Seckler), pp. 20-30. New York: Interscience Publishers.
Silverstein, A. and Joyner, U. (1939). Experimental verification of the theory of oscillating airfoils. *NACA Report 673*.
Smith, M., Wilkin, P. and Williams, M. (1996). The advantages of an unsteady panel method in modeling the aerodynamic forces on rigid flapping wings. *J. Exp. Biol.* **199**, 1073-1083.
Somps, C. and Luttges, M. (1985). Dragonfly flight – novel uses of unsteady separated flows. *Science* **228**, 1326-1329.
Spedding, G. R. and Maxworthy, T. (1986). The generation of circulation and lift in a rigid two-dimensional fling. *J. Fluid Mech.* **165**, 247-272.
Srygley, R. and Thomas, A. (2002). Unconventional lift-generating mechanisms in free-flying butterflies. *Nature* **420**, 600-664.
Sun, M. and Tang, J. (2002). Unsteady aerodynamic force generation by a model fruit fly wing in flapping motion. *J. Exp. Biol.* **205**, 55-70.
Sunada, S., Kawachi, K., Matsumoto, A. and Sakaguchi, A. (2001). Unsteady forces on a two-dimensional wing in plunging and pitching motion. *AIAA J.* **39**, 1230-1239.
Sunada, S., Kawachi, K., Watanabe, I. and Azuma, A. (1993). Fundamental analysis of 3-dimensional near fling. *J. Exp. Biol.* **183**, 217-248.
Theodorsen, T. (1935). General theory of aerodynamic instability and the mechanism of flutter. *NACA Report 496*.
Truesdell, C. (1954). *The Kinematics of Vorticity. Indian University Publications Science Series 19*. Bloomington: Indiana University Press.
Usherwood, J. R. and Ellington, C. P. (2002a). The aerodynamics of revolving wings – I. Model hawkmoth wings. *J. Exp. Biol.* **205**, 1547-1564.
Usherwood, J. R. and Ellington, C. P. (2002b). The aerodynamics of revolving wings – II. Propeller force coefficients from mayfly to quail. *J. Exp. Biol.* **205**, 1565-1576.
VandenBerg, C. and Ellington, C. P. (1997). The three-dimensional leading-edge vortex of a 'hovering' model hawkmoth. *Phil. Trans. R. Soc. Lond. B* **352**, 329-340.
Vogel, S. (1967). Flight in *Drosophila*. III. Aerodynamic characteristics of fly wings and wing models. *J. Exp. Biol.* **46**, 431-443.
Vogel, S. (1994). *Life in Moving Fluids*. Princeton, NJ: Princeton University Press.
Wagner, H. (1925). Über die Entstehung des dynamischen Äuftriebes von Tragflügeln. *Z. Angew. Math. Mech.* **5**, 17-35.
Walker, J. (2002). Rotational lift: something different or more of the same? *J. Exp. Biol.* **205**, 3783-3792.
Walker, J. A. and Westneat, M. W. (2000). Mechanical performance of aquatic rowing and flying. *Proc. R. Soc. Lond. Ser. B. Biol. Sci.* **267**, 1875-1881.
Walker, P. B. (1931). Experiments on the growth of circulation about a wing and an apparatus for measuring fluid motion. *Rep. Memo. Aeronaut. Res. (Great Britain) No 1402*.
Wang, Z. J. (2000). Two dimensional mechanism for insect hovering. *Phys. Rev. Lett.* **85**, 2216-2219.
Weis-Fogh, T. (1973). Quick estimates of flight fitness in hovering animals, including novel mechanisms for lift production. *J. Exp. Biol.* **59**, 169-230.
Wilkin, P. J. and Williams, M. H. (1993). Comparison of the instantaneous aerodynamic forces on a sphingid moth with those predicted by quasi-steady aerodynamic theory. *Physiol. Zool.* **66**, 1015-1044.
Willmott, A. and Ellington, C. (1997a). The mechanics of flight in the hawkmoth *Manduca sexta*. 2. Aerodynamic consequences of kinematic and morphological variation. *J. Exp. Biol.* **200**, 2773-2745.
Willmott, A. P. and Ellington, C. P. (1997b). Measuring the angle of attack of beating insect wings: robust three-dimensional reconstruction from two-dimensional images. *J. Exp. Biol.* **200**, 2693-2704.
Wu, J. (1981). Theory for aerodynamic force and moment in viscous flows. *AIAA J.* **19**, 432-441.
Zanker, J. M. and Gotz, K. G. (1990). The wing beat of *Drosophila melanogaster* II. Dynamics. *Phil. Trans. R. Soc. Lond. B* **327**, 19-44.
Zbikowski, R. (2002). On aerodynamic modelling of an insect-like flapping wring in hover for micro air vehicles. *Phil. Trans. R. Soc. Lond. Ser. A. Math. Phys. Eng. Sci.* **360**, 273-290.